Extreme Mechanics Letters 71 (2024) 102199

Contents lists available at ScienceDirect

Extreme Mechanics Letters

journal homepage: www.elsevier.com/locate/eml

Transition waves in bistable systems generated by collision of moving breathers

A. Paliovaios [a,b], G. Theocharis [a], V. Achilleos [a], V. Tournat [a,*]

[a] Laboratoire d'Acoustique de l'Université du Mans (LAUM), UMR 6613, Institut d'Acoustique - Graduate School (IA-GS), CNRS, Le Mans Université, France
[b] Section of Condensed Matter Physics, National and Kapodistrian University of Athens, University Campus, GR-157 84 Athens, Greece

ARTICLE INFO

Keywords:
Nonlinear mechanical waves
Multi-stable metamaterials
Transition waves
Dynamic reconfiguration
Traveling breathers

ABSTRACT

Mechanical metamaterials with multistability can support transition waves, propagation fronts that change the state of the material as they progress, and thus confer reconfigurability. The next step is to control where and when the transition wave is triggered. In this work, motivated by the existence of discrete breathers in Klein–Gordon lattices, we demonstrate that colliding moving breathers are able to trigger transition waves in bistable mechanical systems. We numerically generate counter-propagating breathers using drivers located at both ends of a finite bistable lattice, and when they collide, transition fronts can be formed. Our study reveals that fine-tuning the generated breathers allows us to control where the transition front forms in the system, and enables complex collision and transition wave triggering scenarios. The parameters of the system considered have been chosen according to experimental works on bistable lattice models under the presence of an asymmetric bistable on-site potential. Consequently, the method we propose for the remote generation of transition waves offers a new way of finely controlling the reconfiguration of mechanical systems with multiple equilibrium states.

1. Introduction

Bistability or even multistability is very common in nature. It is used and can be found in a great variety of systems and is a key ingredient across scales and processes, e.g. dislocations in crystal lattices [1–4], domain walls in magnetic systems [5–8], structural phase transitions [9–11], solitons in polyacetylene [12] or DNA [13,14], micromechanical systems [15,16], buckled beams [17,18], just to name a few.

All these examples share common features regarding the theoretical tools used to describe the processes arising from bistability. Recently, flexible mechanical metamaterials (FlexMMs) [19], which can be defined as artificial, architected structures possessing the ability to deform substantially, repeatedly and reversibly [20], are the subject of an important scientific interest for several reasons, (i) the great variety of structures that can now be fabricated, (ii) the new modeling and simulation tools to describe their behavior, (iii) the range of applications in engineering and beyond. Indeed, advanced manufacturing techniques, such as multimaterial additive manufacturing, additive 3D polymer printing and laser cutting [21], are now widely available, giving the opportunity to design mechanical metamaterials with, e.g., negative Poisson's ratio [22,23], negative thermal expansion [24], negative compressibility [25], negative density or mass [26] and topologically protected states [27–29]. These extreme or fine properties have potential uses and applications [30,31], e.g., as programmable structures [32], soft robots [33–35], energy harvesters [36–38], energy absorbers [39] and mechanical logic devices [40].

Among the others, FlexMMs which are able to support non-linear waves can also be manufactured [41] and accurately modeled. For example, vector solitons [42] and their collisions [43] have been analyzed in systems with coupled rotational and translational degrees of freedom, rarefaction solitary waves [44,45] in strain-softening materials, solitary waves in systems with bistable coupling elements [46] or bistable on-site potential [47] and transition waves in multi-stable systems [48–52]. The latter non-linear waves, of particular interest here, are transition waves or wavefronts that can propagate along a lattice exhibiting multistability. They separate domains which are in distinct stable states, representing as such a reconfiguration front of the FlexMM. Because of this, controlling in space and time the generation and the spreading of transition waves in FlexMM paves the way for the controllable mechanical reconfiguration of advanced structures.

Until now, despite the numerical, analytical and experimental investigation on non-linear FlexMMs, there is a lack of understanding of

* Corresponding author.
E-mail address: vincent.tournat@univ-lemans.fr (V. Tournat).

https://doi.org/10.1016/j.eml.2024.102199
Received 29 October 2023; Received in revised form 31 May 2024; Accepted 30 June 2024
Available online 10 July 2024

their dynamic response under modulated wave excitations, such as vibrations induced by drivers at a given position of the sample which is a common experimental technique to excite a structure. Furthermore, the generation of transition waves is most often induced quasi-statically, and their dynamics or spatio-temporally controllable generation stays almost unexplored. As a consequence, the high level of control that multistable FlexMMs offer cannot be fully exploited. Nevertheless, from the existing studies it is demonstrated that in order to produce transition waves, large amplitude excitations (local deformations of 30%–50%) are usually required [49–52].

It has also been reported that transition waves can be triggered remotely, within a multi-stable chain of rotating units and not only at its boundary, by the collision of two counter-propagating solitons generated at both ends of the multi-stable FlexMM [53]. These pulse solitons, analogous to KdV solitons, have a spatial extent of 5-10 unit-cells of the FlexMM and whether or not they nucleate a transition wave upon collision mostly depend on their amplitude (or equivalently energy, or velocity, or width), via a threshold effect. A step forward has recently been taken in the same vein by analyzing a two-dimensional collision configuration of these impulse solitons, offering richer collision scenarios and results [53]. Interestingly, some of the systems studied earlier for transition waves are nonlinear Klein–Gordon lattices [21], known as well to support envelope solitons [54]. Consequently, the questions we ask are the following: can we make use of the collision of robust modulated waves such as envelope solitons to trigger transition waves in multi-stable nonlinear Klein–Gordon lattices, and what are the collision conditions to achieve transition wave nucleation?

Therefore, in the present article, we consider a one-dimensional Klein–Gordon model and, starting from the existence of intrinsic localized propagating modes in non-linear lattices, we show that under certain conditions, their collisions can trigger the generation of transition waves. In addition, to allow for an experimentally realizable configuration, we produce these modes using drivers located at the extremities of the chain. Because the drivers can be activated at controlled times, excited wave-packets can collide at different locations in the lattice, allowing us to control the excitation of transition waves in space.

The remainder of this article is organized as follows. In Section 2 starting from the discrete model under consideration and the corresponding equations of motion, we present the necessary linear and non-linear wave properties of the system. Then, we proceed to the presentation of the method we use in order to study numerically our system. In Section 3 we apply our method to a specific lattice whose parameters provide the desired dynamical response, and are selected in light of theoretical criteria defining the properties of moving discrete breathers as discussed in Section 2. Because we use dimensionless parameters, they can easily be adjusted in order to capture the dynamics of already existing structures. Finally, we point out the conditions under which a transition wave triggering can occur, providing a systematic procedure for its spatio-temporal control. The last section is a summary of our findings and some remarks on the experimental investigation of our numerical results.

2. Theory

2.1. Description of the system and its linear properties

In the present work we are interested in a chain of coupled mechanical elements as shown in Fig. 1 . This configuration is inspired by experimental settings in [49,50] that support transition waves. In particular, we consider that each element consists of a mass that is located at the middle of a buckled elastic beam indicated by thick solid curves in Fig. 1. Analysis of the potential energy produced by such buckled beams shows that the on-site bi-stable potential can be approximated by a polynomial function of displacement [50]. The bistable mechanical elements are coupled to their neighbors through linear longitudinal springs. Masses are able to move along the horizontal direction only, i.e. longitudinal displacements are considered.

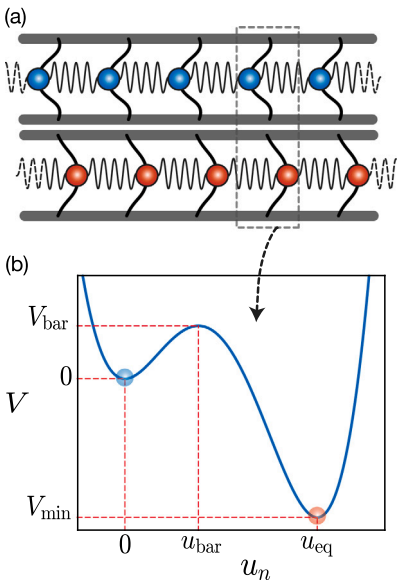

Fig. 1. (a) Schematic representation of the considered chain of linearly coupled bistable elements. The filled circles represent the masses and the curved black lines the buckled beams that are bistable. (b) The potential produced by the buckled beams and described by Eq. (2) for $V_2 > 0$. The blue and the red filled circles correspond to masses placed in the local and the global equilibrium point of the potential, respectively. (For interpretation of the references to color in this figure legend, the reader is referred to the web version of this article.)

The Hamiltonian of such system, neglecting the losses, can be written as,

$$\mathcal{H} = \sum_{n=0}^{N-1} \left[\frac{m}{2}\dot{u}_n^2 + \frac{G}{2}(u_{n+1} - u_n)^2 + V(u_n) \right], \tag{1}$$

where u_n is the relative displacement of each mass n from its equilibrium position, m is the mass, G is the stiffness of coupling springs between neighboring masses and $V(u_n)$ is an on-site asymmetric bistable potential given by the following expression [49],

$$V(u_n) = \left(\frac{V_1 u_n^2}{2} - \frac{V_2 u_n^3}{3} + \frac{V_3 u_n^4}{4} \right), \tag{2}$$

where $V_{1,2,3}$ are constants defining the potential's strength and shape (Fig. 1). If $V_1, V_3 > 0$ and $V_2^2 > 4V_3V_1$, the potential has two stable equilibrium points at

$$u_{\text{eq}} = \left\{ 0, \frac{V_2}{2V_3} + \sqrt{\frac{V_2^2}{4V_3^2} - \frac{V_1}{V_3}} \right\}, \tag{3}$$

which are separated by an energy barrier

$$V_{\text{bar}} = \frac{1}{12}(3V_1 + V_2 u_{\text{bar}})u_{\text{bar}}^2, \tag{4}$$

located at

$$u_{\text{bar}} = \frac{V_2}{2V_3} - \sqrt{\frac{V_2^2}{4V_3^2} - \frac{V_1}{V_3}}. \tag{5}$$

The Hamiltonian of Eq. (1) leads to the following equation of motion for each mass n,

$$m\frac{d^2u_n}{dt^2} = G(u_{n+1} + u_{n-1} - 2u_n) - (V_1 u_n - V_2 u_n^2 + V_3 u_n^3). \tag{6}$$

Introducing the following dimensionless quantities,

$$T = \sqrt{\frac{G}{m}}t = \omega_0 t,\ U_n = \frac{V_2 u_n}{V_1},$$
$$\lambda^2 = \frac{V_1}{G} \text{ and } \beta = \frac{V_1 V_3}{V_2^2}, \tag{7}$$

we can simplify Eq. (6) into,

$$\frac{d^2U_n}{dT^2} = (U_{n+1} + U_{n-1} - 2U_n) - \lambda^2(U_n - U_n^2 + \beta U_n^3). \tag{8}$$

In the linear limit the equations of motion are written as,

$$\frac{d^2U_n}{dT^2} = (U_{n+1} + U_{n-1} - 2U_n) - \lambda^2 U_n, \tag{9}$$

which is the well-known discrete Klein–Gordon equation possessing the following linear dispersion relation,

$$\omega(ka) = \sqrt{\lambda^2 + 4\sin^2\frac{ka}{2}},\ ka \in [0, \pi], \tag{10}$$

where a is the lattice period and ka is considered as the normalized wavenumber. From Eq. (10) we see that the linear spectrum is confined within a single band with frequencies $\omega \in [\lambda, \sqrt{\lambda^2+4}]$.

2.2. Non-linear solutions of the system — discrete breathers

Among the various solutions of Eq. (8), we focus here on the discrete breathers [55,56], namely time-periodic and spatially localized nonlinear solutions, for which the central ω_{br} and all the higher-harmonic frequencies $n\omega_{\text{br}}$ lie outside of the linear spectrum. This determines a minimum value for the on-site potential's strength of $\lambda > \sqrt{4/3}$ for which $2\omega_{\text{br}} > \sqrt{\lambda^2+4}$.

In contrast to breathers of continuous wave equations, we note that in discrete lattices, because of the broken continuous translational symmetry, discrete breathers can propagate only under specific conditions [57,58]. The latter can usually be interpreted using a Peierls–Nabarro potential [59], but can also be interpreted through the strength of discrete effects. The properties of moving breathers have been studied in various contexts including Fermi–Pasta–Ulam–Tsingou lattices [60], Peyrard–Bishop model for DNA [61], mass dimers [62], Klein–Gordon lattices [63,64] and discrete non-linear Schrödinger models [65–67]. In addition, their collisions have been studied for several systems including Klein–Gordon lattices [63,64] and discrete non-linear Schrödinger models [65–68]. However, in context of bistable FlexMMs for which the lump-element approach corresponds to a Klein–Gordon lattice with asymmetric on-site potential, see Eq. (9), there is no previous study on the existence, mobility or collision of discrete breathers to the best of our knowledge.

2.3. Numerical approach

Here we describe the methodology to obtain discrete breathers of Eq. (9) numerically. For a discrete breather of a given period $T_{\text{br}} = 2\pi/\omega_{\text{br}}$, we find solutions of the following set of equations

$$\mathbf{X}[T_{\text{br}}; \mathbf{X}(0)] - \mathbf{X}(0) = 0, \tag{11}$$

where $\mathbf{X}(T) = [U_1(T) \cdots U_N(T)\ \dot{U}_1(T) \cdots \dot{U}_N(T)]^T$ and $U_n, \dot{U}_n$ satisfy

$$\begin{cases} \dfrac{dU_n}{dT} = \dot{U}_n \\ \dfrac{d\dot{U}_n}{dT} = (U_{n+1} + U_{n-1} - 2U_n) - \lambda^2(U_n - U_n^2 + \beta U_n^3). \end{cases} \tag{12}$$

This set of equations can be solved iteratively using a Newton–Raphson method using a sufficiently good initial guess. In order to have such an initial guess, we follow Ref. [54], focusing on slowly varying standing envelope solutions at $k = 0$ and correspondingly with $\omega = \lambda$, having the form

$$U_n(T) = \varepsilon F e^{-i\lambda T} + 2\varepsilon^2|F|^2 - \frac{\varepsilon^2}{3}F^2 e^{-2i\lambda T} + \text{c.c.}, \tag{13}$$

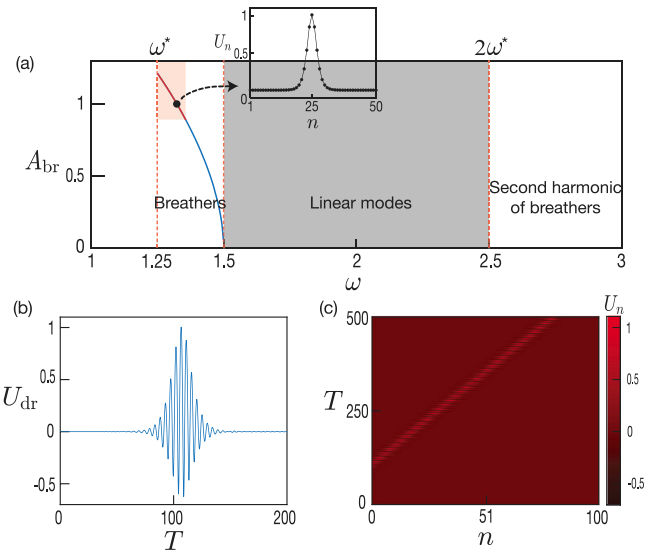

Fig. 2. (a) Frequency regimes where breathers, linear modes and breather's second harmonic are predicted. The breather's amplitude A_{br} as function of frequency is also depicted. In the inset, the spatial profile of a breather with frequency $\omega_{\text{br}} = 1.32$ (black marker) is shown. (b) Time evolution of the displacement imposed to a driven unit to excite the breather. (c) Propagation along a lattice of $N = 101$ elements of the moving breather produced by the driving profile depicted in (b). The breather's characteristics are $(A_{\text{br}}, \omega_{\text{br}}, qa) = (1.00, 1.32, 0.3)$.

where ε is an arbitrary small parameter and F is a slow varying envelope.

In particular we consider that $F = F(\tau, \xi)$ where $\tau = \varepsilon^2 T$, $\xi = \varepsilon n a$ are the slow time and the continuous space variable respectively. Using this approach and the multiple scales method, F satisfies the following non-linear Schrödinger equation (NLS) [54]

$$i\frac{\partial F}{\partial \tau} + P\frac{\partial^2 F}{\partial \xi^2} + Q|F|^2 F = 0, \tag{14}$$

where the parameters P, Q are given by

$$P = \frac{a^2}{2\lambda},\ Q = \frac{\lambda}{6}(10 - 9\beta). \tag{15}$$

For our systems parameters a, β, λ, we have $PQ > 0$, which corresponds to the so-called focusing NLS equation admitting the following bright soliton solution [54],

$$F(\tau, \xi) = \text{sech}\left(\sqrt{\frac{Q}{2P}}\xi\right)e^{i\frac{Q}{2}\tau}. \tag{16}$$

The solutions obtained using Eqs. (13) and (16) provide a good initial guess for the Newton–Raphson iterative method and are expected to converge to localized breathers with frequencies ω_{br} below (but close to) the low-frequency limit of the linear mode band, due to the softening non-linearity. Higher amplitude solutions and their stability can be obtained by performing a continuation on the breathers frequency ω_{br} and Floquet linear stability analysis (see Appendix for the stability diagram and the details).

The amplitude dependence on the possible breather's frequency is depicted in Fig. 2(a). For this figure and all the figures presented afterwards the lattice parameters are set equal to $\beta = 0.2$ and $\lambda = 1.5$. This choice is reasonable since $\beta = 0.2$ is an experimentally measured value [49] and $\lambda = 1.5$ ensures that discrete effects are not strong and non-radiative breathers exist. In Fig. 2(a) it is shown that for the chosen parameters, breathers with the second harmonic above the linear frequency band exist for $\omega^* < \omega_{\text{br}} < \lambda$.

The obtained discrete breathers are stationary and thus not suitable for our purpose. In order to obtain a moving discrete breather we make

use of the following ansatz (see [64]),

$$U_n(T=0) = U_S \cos[qa(n-n_0)],$$
$$\dot{U}_n(T=0) = U_S \sin[qa(n-n_0)], \tag{17}$$

where qa is a free parameter and U_S is the spatial profile of the standing breather we obtained. For different values of qa, a breather can propagate with different velocities v_{br}.

Having in mind usual experimental constraints, we want to mimic the experimental excitation of moving discrete breathers using external drivers located at the two extremities of the finite structure. In order to obtain a driving profile U_{dr}, we let a moving breather propagate and we keep record of an element's displacement as function of time. This driving profile can be used in order to excite a moving breather with amplitude A_{br}. In Fig. 2(b) we depict a driving profile obtained in order to generate the moving breather of Fig. 2(c) which propagates along the lattice. In the above simulations of the flexMM, the equations of motion Eq. (8) are integrated with a 4th order Runge–Kutta method.

3. Moving breathers and transition waves

Our first objective is to trigger transition waves by the collision of moving breathers generated by drivers at the extremities of the flexMM, as it is depicted in the left panel of Fig. 3. For simplicity, in the rest of the article we focus on collisions of identical moving breathers, i.e. they have the same amplitude and velocity. In the right panel of Fig. 3, we illustrate the different stages of this collision and triggering process; starting with a configuration for which all the bistable elements are in the first stable equilibrium (see blue points and $U_n = 0$), the system ends up with all the bistable elements oscillating around the second stable equilibrium (see orange points and $U_n \simeq 3.6$).

In particular, the system is first driven at its two boundaries using the signal obtained by the method described in Section 2.3 which generates two counter-propagating breathers moving along the lattice. When the breathers collide, a structural reconfiguration may be triggered and two transition fronts start to propagate apart, as visible in Fig. 3. The propagation of these fronts then gradually switch the bistable elements towards the second stable configuration.

In the following, we present in details the conditions under which this reconfiguration takes place. In general, our study reveals that the generation of transition waves can be controlled by three parameters: (i) *the breather amplitude* A_{br}, (ii) *the relative phase difference* of moving breathers at the moment of the collision $\Delta\Phi_0$ and (iii) the phase of moving breathers at the moment of collision, which we denote as *collision phase*. Regarding the breather's amplitude dependence, we numerically found the threshold ($A_{br} > 0.92$) beyond which the triggering is possible, highlighted by the red shaded area in Fig. 2(a), and similar to what has been recently reported for long-wavelength soliton collision [53]. In the next subsections, we focus on the other two parameters.

3.1. Effect of relative phase difference

In the context of discrete non-linear Schrödinger systems, it is known that the outcome of the collision of discrete breathers crucially depends on their relative phase. Yet, among the different interactions possible, we focus here on the attractive and the repulsive ones, because the first can lead to the formation of transition fronts and the second gives us the ability to change the direction of breathers motion upon reflection with negligible radiation. In particular, the interaction can be attractive and highly inelastic for in-phase breathers, or repulsive and almost elastic for out-of-phase breathers [69]. We note that the collision of non-linear waves in discrete systems is in general inelastic. Only discrete systems with special discretizations (e.g. Ablowitz–Ladik model) can host elastic collisions.

In our case, a relative phase between the two discrete breathers can be induced by an arbitrary time delay between the two drivers. When two identical breathers are generated with a time difference ΔT_0, their relative phase is equal to

$$\Delta\Phi_0 = \omega_{br}\Delta T_0. \tag{18}$$

Figs. 4(a), (c) show that in-phase moving breathers ($\Delta\Phi_0 \bmod 2\pi = 0$) create a high amplitude excitation during collision due to their mutual attractive interaction. We notice that this high amplitude excitation does not always lead to the triggering of transition waves [see Fig. 4(c)]. On the contrary, Fig. 4(b) shows that out-of-phase moving breathers ($\Delta\Phi_0 \bmod 2\pi = \pi$) interact repulsively. These observations are in agreement with the literature on discrete NLS systems [69] and Klein–Gordon lattices [63,64].

3.2. Effect of collision phase

We have shown up to now that the triggering of transition waves using identical moving breathers requires: (i) a certain breathers amplitude threshold and (ii) the breathers to be in-phase. However, Fig. 4 indicates that there is one more parameter to be considered, the collision phase.

Let us first assume that we simultaneously excite two counter-propagating identical breathers with a relative distance

$$\frac{d}{a} = (N-1). \tag{19}$$

By construction, their collision occurs at the center of the lattice, which is either at one site or in between two sites depending on the odd or even number of units, and the only parameter that may influence the collision outcome is the phase of the breathers at the collision point. To investigate the effect of this collision phase, we perform simulations using various lattice lengths, thus changing the collision time and in turn the collision phase. An estimation of the collision phase can be sought as follows: the time needed for a single breather to move by one site is $\Delta T_1 = 1/v_{br}$. Thus the phase shift of the breather arriving at the center of the lattice, due to the propagation over $N/2$ lattice points, is $N\omega_{br}/2v_{br}$. However, an extra phase shift is expected due to the interaction which cannot be described analytically. Thus we study the role of the collision phase on the outcome of the collision numerically.

Such a numerical qualitative analysis is illustrated in Fig. 5 where different collision outcomes are reported for different lattice lengths. In general, and for all explored moving breathers, we observe three main outcomes. On the one hand, panel (a) (with $N = 66$) and (c) (with $N = 68$) of Fig. 5, show the case where the collision outcome consists of two counter-propagating localized wavepackets. On the other hand, for $N = 67$ in panel (b), a different outcome is a non-traveling localized oscillation formed at the collision point. In both the aforementioned scenarios, we observe the generation of additional low-amplitude waves due to the inelastic collision. The most relevant outcome, for our purposes, is shown in Fig. 5(d) where after the collision of the breathers, a transition wave is formed and at finite times all the elements migrate and oscillate around the global minimum of the potential.

In Fig. 6 we present the outcome of in-phase moving breathers collision for three values of the time difference ΔT_0 (or relative phase) and two values of lattice length (or collision time). We observe that a shift of time difference equal to $2T_{br}$ leads to the same collision outcome. This periodic behavior in ΔT_0 can be explained by considering the time of collision for two counter-propagating breathers in a lattice of N elements (neglecting again effects of the interaction of breathers),

$$T_* = \frac{N-1}{2v_{br}} + \frac{\Delta T_0}{2}, \tag{20}$$

taken from the generation time of the first breather. Given that the phase of a breather at the collision time is $\Phi_{br} = \omega_{br}T_*$, for a given lattice and a given breather, this phase only varies because of ΔT_0. In order to recover the same collision outcome, the collision phase

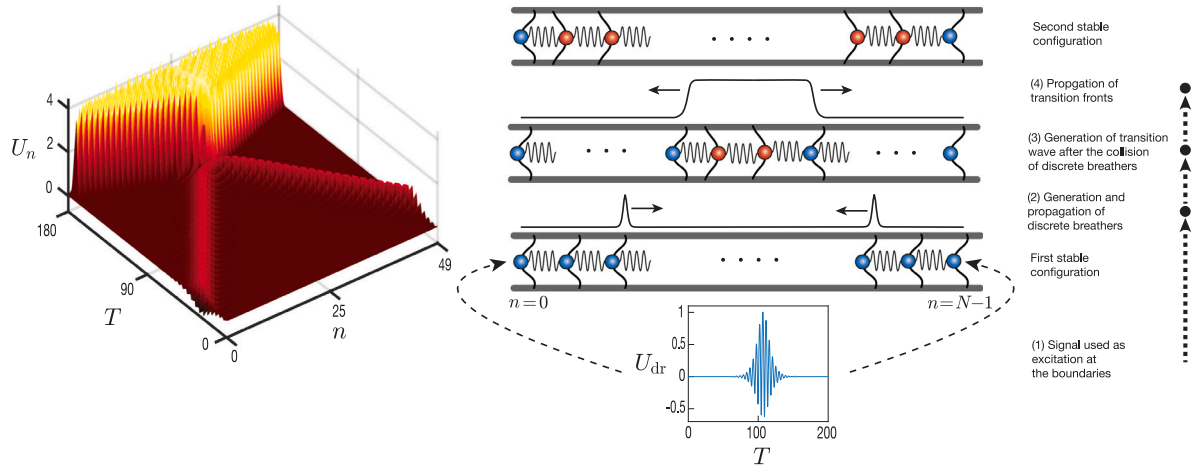

Fig. 3. Schematic illustration of the proposed mechanism to trigger transition waves. Two drivers located at the boundaries generate counter-propagating high amplitude breathers. Their collision leads to a high amplitude local excitation which can trigger a transition wave.

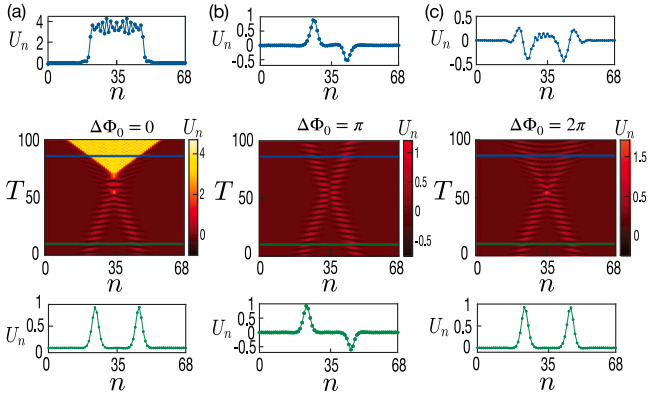

Fig. 4. Identical breathers with amplitude $(A_{\rm br}, \omega_{\rm br}, qa) = (0.95, 1.339, 0.32)$ and relative phase difference (a) $\Delta\Phi_0 = 0$, (b) $\Delta\Phi_0 = \pi$ and (c) $\Delta\Phi = 2\pi$, respectively, counter-propagating in a lattice of $N = 69$ elements. In (b) a nearly elastic collision is observed in contrary to (a) and (c) in which radiation and high-amplitude excitations are generated. The vertical lines correspond to the spatial profile of system as depicted in the panels.

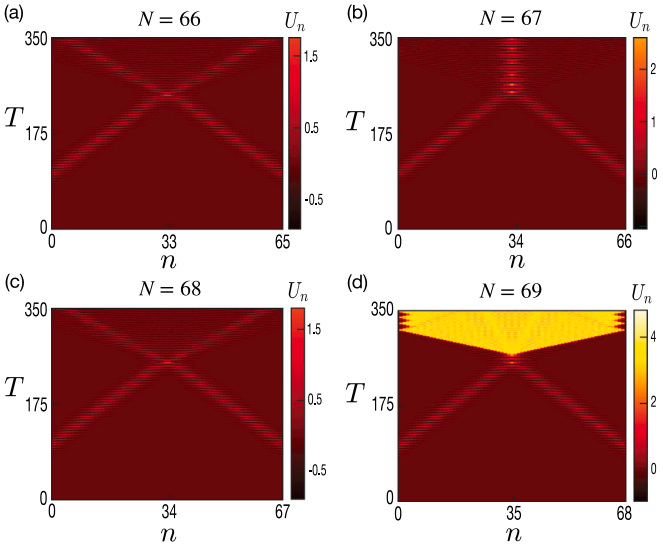

Fig. 5. Two in-phase breathers with $(A_{\rm br}, \omega_{\rm br}, qa) = (0.95, 1.339, 0.32)$ counter-propagate and collide within lattices with different lengths. The breathers' parameters are chosen such as $v_{\rm br} \approx \omega_{\rm br}/2\pi$. In (a) and (c) the formation of new counter-propagating localized wave-packets is observed. In (b) and (d) energy trapping and formation of transition fronts, respectively, are observed indicating that depending on the phase, the outcome can significantly change.

should be the same modulo 2π, corresponding in turn to a period of $4\pi/\omega_{\rm br} (= 2T_{\rm br})$ for ΔT_0. This period for the breather phase at the collision is reflected in the outcome of the transition wave triggering as observed in Fig. 6.

The main conclusion of Fig. 6 is that if a transition wave does not occur for a breather collision with a given ΔT_0, then a $2\pi/\omega_{\rm br}$ shift in time difference should lead to the triggering of a transition wave. In other words, a transition wave can always be triggered with the collision of in-phase high-enough amplitude moving breathers, if the time difference ΔT_0 is appropriately tuned.

3.3. Controllability of phase transitions

Until now, we have considered only small time differences $\Delta T_0 \in [0, 2T_{\rm br}]$ between the breathers, which leads to collisions close to the center of the lattice. However, taking into consideration the findings presented in Section 3.2, we can expect that a transition can be triggered if we increase this small time difference by multiple integers of $2T_{\rm br}$. In fact a time delay equal to $\Delta T_0 + 4m\pi/\omega_{\rm br}$, $m \in \mathbb{Z}$, is ensured to give a transition wave, where $\Delta T_0 \in [0, T_{\rm br}]$ is a small time difference leading to transition. To roughly estimate the point of the collision, we consider identical breathers as point masses counterpropagating

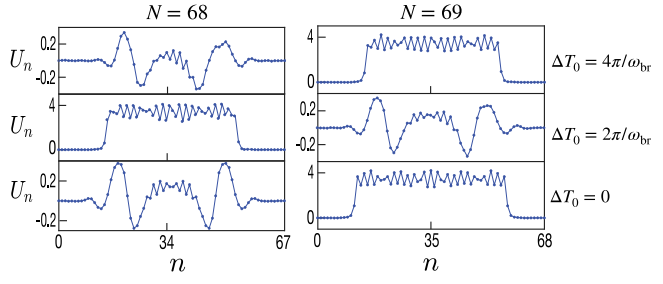

Fig. 6. Snapshots of displacements U_n in a lattice consisting of $N = 68$ elements (left panel) and $N = 69$ (right panel), respectively, after the collision of identical breathers with amplitude $(A_{\rm br}, \omega_{\rm br}, qa) = (1.00, 1.32, 0.32)$. The breathers have been generated with time difference ΔT_0 and counter-propagate. From down to top the time difference equals to $\Delta T_0 = \{0, T_{\rm br}, 2T_{\rm br}\}$, respectively. We show that a transition wave is always triggered if we appropriately tune the time difference ΔT_0. As observed, the tuning depends on the lattice length.

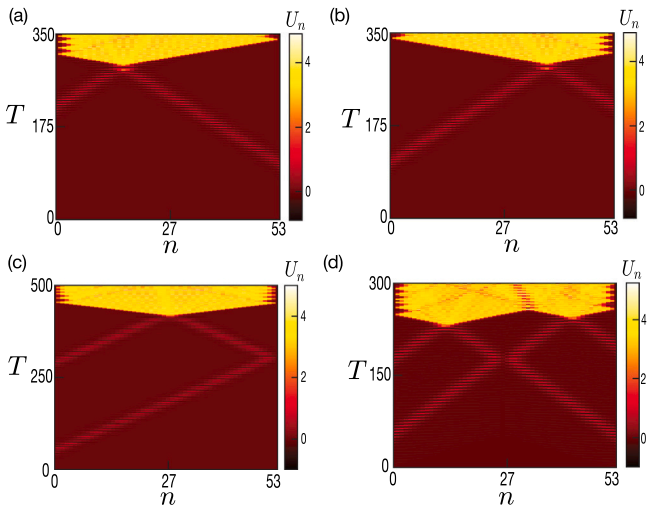

Fig. 7. (a),(b) Transition waves triggered by identical breathers on a lattice of $N = 54$ elements. By fine-tuning the time delay between their generation, different the transition fronts are generated in different lattice points. (c) Transition wave generated after the reflection of a moving breather on the boundary. (d) Multiple transition waves generated on a lattice of $N = 54$ elements. All the breathers used are characterized by $(A_{\rm br}, \omega_{\rm br}, qa) = (1.00, 1.32, 0.3)$.

with constant velocity $v_{\rm br}$. Under this description and the chosen time difference, we get

$$n_{\rm c} = \frac{N-1}{2} \pm \left(\frac{2m\pi v_{\rm br}}{\omega_{\rm br}} + \frac{v_{\rm br}\Delta T_0}{2} \right). \tag{21}$$

where $+/-$ corresponds to the activation of left/right driver first.

Therefore, we can tune the time difference in order to trigger a transition wave at different locations, a mechanism depicted in Figs. 7(a) and (b).

Going a step further we demonstrate that using breathers generated by drivers allows a plethora of controllable colliding events. By generating multiple breathers, we can produce multiple transition waves in different positions and/or at different moments. This is possible if we take advantage the collision of out-of-phase breathers or of the reflections at boundaries.

In Figs. 7(c) and (d) we give such examples. In Fig. 7(c) we use a single driver placed on the left boundary exciting two delayed breathers. After the reflection of the first generated moving breather on the right boundary, a collision occurs with the second generated breather leading to a transition. In Fig. 7(d) two drivers are placed on opposite boundaries and generated both two delayed breathers. By producing a first pair of breathers which collide nearly elastically, we make them move in opposite directions after the collision and by carefully choosing when the second pair of breathers is generated, two transition waves in different spatiotemporal points are triggered in the lattice.

3.4. Effect of losses

In FlexMMs dissipative effects usually cannot be neglected. Nevertheless, the dissipative properties of FlexMMs can be modified to some extent by the geometry of the flexible elements, the choice of materials and the type of interaction between neighboring elements. In order to qualitatively evaluate the effect of dissipation on the propagation of breathers in bistable structures, we consider the following linear viscous force, $-\Gamma \frac{du_n}{dt}$.

By introducing this dissipative term in Eq. (8) we get

$$\frac{d^2U_n}{dT^2} + \gamma \frac{dU_n}{dT} = (U_{n+1} + U_{n-1} - 2U_n) - \lambda^2(U_n - U_n^2 + \beta U_n^3), \tag{22}$$

where γ is the normalized damping coefficient $\gamma = \omega_0 \Gamma / G$.

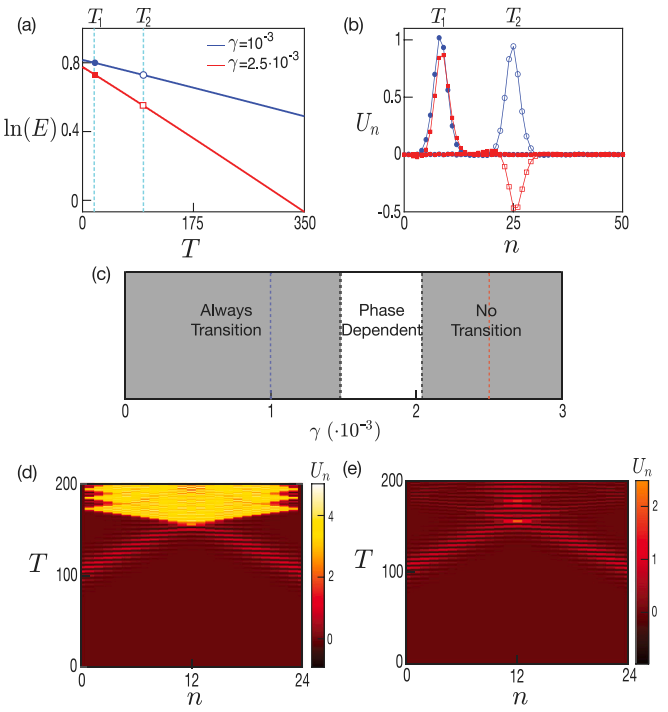

Fig. 8. The breather generated by drivers has $(A_{\rm br}, \omega_{\rm br}, qa) = (1.1, 1.29, 0.3)$ for all the figures. (a) Logarithm of energy as function of time for $\gamma = 10^{-3}$ and $\gamma = 5 \cdot 10^{-3}$. (b) The spatial profiles of a breather at different moments given by the vertical dashed line in (a) for the two damping coefficients. (c) Possibility of transition waves generation in a lattice with $N = 25$ elements as function of γ. The blue and red dashed lines correspond to $\gamma = 10^{-3}$ and $\gamma = 2.5 \cdot 10^{-3}$, respectively. (d),(e) Time evolution of a system with $N = 25$ elements with two counter-propagating identical breathers generated by drivers at $n = 0$ and $n = 24$ for $\gamma = 10^{-3}$ and $\gamma = 2.5 \cdot 10^{-3}$, respectively. (For interpretation of the references to color in this figure legend, the reader is referred to the web version of this article.)

Losses change the wave propagation in several ways. Except from the well-known energy loss and the corresponding decrease in amplitude, the dissipation also adds a phase shift to the breather oscillations. In view of these considerations, the damping coefficient γ is chosen to be very low. To understand these effects in our system, in Fig. 8 we show how the dissipation affects the breathers propagation and the triggering of transition waves upon collision, for different damping coefficients.

In Fig. 8(a) the logarithm of energy as function of time is depicted. Notably, the logarithm decays linearly indicating an exponential decay of energy as function of time with a decay rate equal to the damping coefficient. In Fig. 8(b) we show the spatial profile of the lattice displacements at two different moments (vertical dashed lines of Fig. 8(a)) after the initial breather has propagated for some distance. In both cases the breather is the same and was generated at $n = 0$ by a driver. In this figure the two major effects of dissipation, the amplitude decay and the phase shift, are demonstrated since at the given moments with identical initial breather, waves with different profiles are observed for different damping coefficients.

As a consequence, in Fig. 8(c), we show that for different damping coefficients we have different collisions characteristics. Specifically, three regimes are reported. In the first one, the phase shift and the amplitude decay are small enough and do not change the outcome of the collision. In the second regime, the phase shift is able to change the outcome of collisions depending on the value of damping coefficient. As it has been already highlighted in this work, the phase can affect the collision. Specifically, consider two lattices with the same length and different damping coefficients $\gamma_1 > \gamma_2$ along which identical breathers propagate. If the damping coefficients belong to this regime, even

though the energy at the moment of the collision is lower, it is possible to observe the generation of a transition wave in the first case, but not in the second. In the third regime of higher damping coefficients, the breathers do not carry enough energy at the collision point to induce a transition. Finally, in Fig. 8(d, e) we illustrate with spatio-temporal plots the collision of two counter-propagating breathers produced by drivers under the effect of dissipation (damping coefficients in the first and third regimes) and we demonstrate that even in the presence of dissipation it is possible to trigger transition waves if the lattice is relatively short and the damping dissipation below a certain threshold.

4. Summary and conclusions

In summary we have studied the dynamics of high-amplitude discrete breathers in a Klein–Gordon nonlinear lattice describing bistable mechanical metamaterials. Our studies focus on elements with asymmetric bistability where one of the stable configurations is energetically favorable. We show that the collision of counter-propagating breathers result in a rich variety of outcomes, including the triggering of a transition wave, where the elements of the lattice progressively switch to the other stable configuration. Using a systematic analysis of the collision dynamics we reveal the necessary conditions that lead to the generation of transition waves. More importantly we illustrate that a very fine control of the time and position of the transition wave can be achieved using the breather collisions. For a complete understanding of the phenomenon we also studied the effect of weak dissipation and found that although the collision outcome varies, the triggering of transition wave is still valid. Therefore, our study takes a step to the direction of remotely controllable reconfiguration of bistable systems using vibrations.

Finally, it is worth mentioning that the proposed method for finding non-linear waves can be extended to different systems consisting of coupled non-linear elements [70–73] as has already been pointed out in recent works [74,75]. Moreover, for systems with multistable coupling elements that support solitary waves [76–78] collisions of them may be able to trigger transition waves. In general, collision-induced transition waves lead to large-scale re-configurations and thus to the manipulation of the band structure [70,71,79].

CRediT authorship contribution statement

A. Paliovaios: Conceptualization, Investigation, Visualization, Writing – original draft, Writing – review & editing. **G. Theocharis:** Conceptualization, Formal analysis, Investigation, Methodology, Supervision, Validation, Writing – original draft, Writing – review & editing, Funding acquisition. **V. Achilleos:** Conceptualization, Formal analysis, Investigation, Methodology, Supervision, Validation, Writing – original draft, Writing – review & editing. **V. Tournat:** Conceptualization, Funding acquisition, Investigation, Supervision, Validation, Visualization, Writing – original draft, Writing – review & editing.

Declaration of competing interest

The authors declare that they have no known competing financial interests or personal relationships that could have appeared to influence the work reported in this paper.

Data availability

Data will be made available on request.

Acknowledgment

We acknowledge the support from ANR project ExFLEM ANR-21-CE30-0003-01.

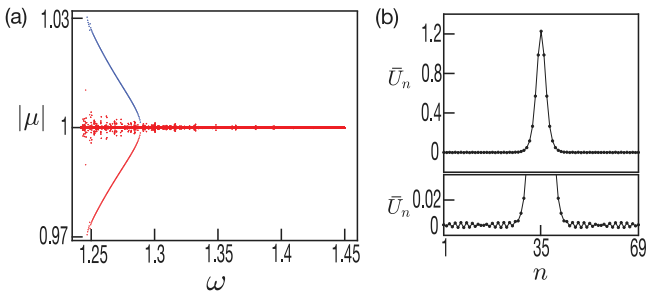

Fig. 9. (a) The Floquet multipliers μ of one-site breather with frequency $\omega \in [1.24, 1.45]$ in a lattice of $N = 69$ elements. Three regimes can be identified. The first is for $\omega \in (1.28, 1.45]$ where only finite size instabilities appear and disappear. The second is for $\omega \in (1.25, 1.28]$ where finite size instabilities coexist with a real instability (blue dots) related with the mobility of discrete breathers. The last one is for $\omega \in [1.24, 1.25]$ where the second harmonic of discrete breather resonates with the linear band and at some point the real instability disappears. (b) A discrete breather with frequency $\omega_{\text{br}} = 1.245$. The resonance with the linear frequency band gives rise to the oscillatory tails. (For interpretation of the references to color in this figure legend, the reader is referred to the web version of this article.)

Appendix. Linear stability analysis of discrete breathers

In order to perform the linear stability analysis of the obtained solutions we use Floquet analysis. We first assume that we have a solution $\bar{U}_n$ of Eq. (8) which we slightly perturb as follows $U_n = \bar{U}_n + \epsilon W_n, \epsilon \ll 1$. Then, substituting it into Eq. (8) and keeping only linear terms of ϵ, we get

$$\frac{d^2 W_n}{dT^2} = (W_{n+1} + W_{n-1} - 2W_n) - \lambda^2 \left(1 - 2\bar{U}_n + 3\beta \bar{U}_n^2\right) W_n. \tag{A.1}$$

As in Section 2.3, we can create a vector $\mathbf{Y}(T) = [W_1(T) \cdots W_N(T)\ \dot{W}_1(T) \cdots \dot{W}_N(T)]^T$ and combining this vector and Eq. (A.1), we can compute the so-called monodromy matrix $\mathcal{F}$ which satisfy the equation

$$\mathbf{Y}(T) = \mathcal{F}\mathbf{Y}(0). \tag{A.2}$$

The eigenvalues $\mu \in \mathbb{C}$ of monodromy matrix are the so-called Floquet multipliers. Because of the Hamiltonian nature of our system, the Floquet multipliers are coming either in real pairs or complex quartets. A Floquet multiplier for which $|\mu| > 1$ indicates the presence of an instability.

The absolute value of the Floquet multipliers is shown in Fig. 9(a). For frequencies $\omega > 1.28$ the unstable Floquet multipliers appear and disappear. This is a known phenomenon which is attributed to finite size effects [80]. Such instabilities disappear in the limit of an infinite chain and do not affect the stability of the obtained solutions. For frequencies $1.25 < \omega < 1.28$ a real instability, which increases as frequency decreases, exists. This instability is related to the mobility of discrete breathers [28]. Finally, for $\omega \leq 1.25$ the resonance of the second harmonic with the linear frequency band (see Section 2.2) gives rise to low amplitude oscillatory tails. A breather inside this resonant regime is plotted in Fig. 9(b).

In Fig. 10(a) and (b) a discrete breather with frequency $\omega_{\text{br}} = 1.26$ and the corresponding Floquet spectrum are plotted, respectively. The inset of Fig. 10(b) indicates the presence of a low amplitude real instability. This is the so-called pinning mode to which the mobility of a discrete breather is attributed and has odd parity as shown in Fig. 10(c), in compliance with the prediction for soft ϕ^4 potentials [28]. Fig. 10(d) shows that indeed this instability can lead to a moving breather by setting the following initial condition $U_n = \bar{U}_n + 0.5W_n$, $\dot{U}_n = 0.5\dot{W}_n$. The perturbation has high amplitude because the unstable Floquet multiplier is relatively weak and as a consequence the time needed in order the instability to be observed is long. Lastly, we should comment on the fact that in our work we did not take advantage of the pinned mode, but we used another perturbation given by Eq. (17). This choice

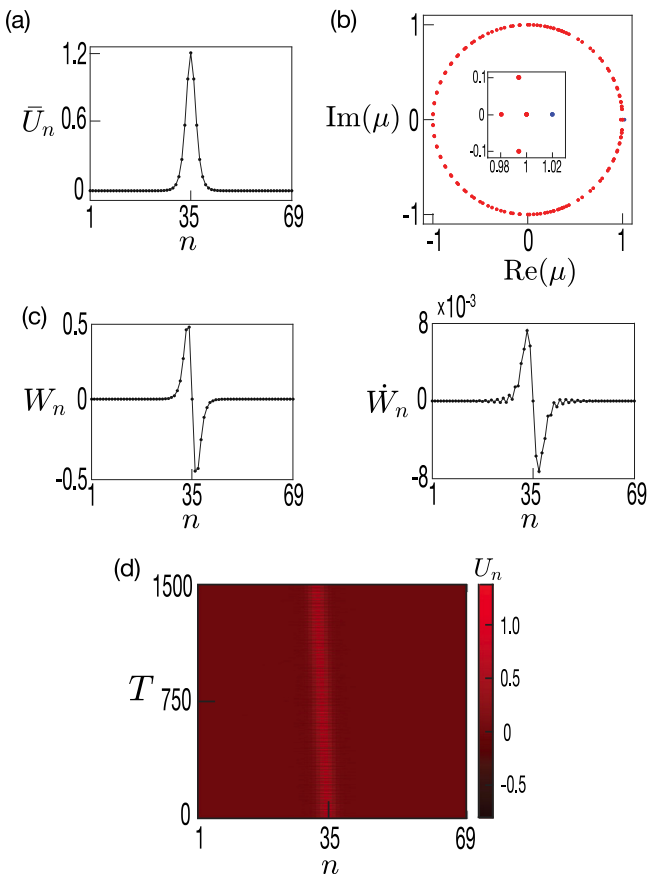

Fig. 10. (a) A discrete breather with frequency $\omega_{br} = 1.26$ and (b) the corresponding Floquet multipliers on the complex plain. The inset indicates the presence of a Floquet multiplier outside the unit circle leading to a real instability. (c) The displacement and velocity profile of the eigenvector which corresponds to the unstable Floquet multiplier of the solution with frequency $\omega_{br} = 1.26$. By perturbing the discrete breather using the eigenvector a moving one is obtained as can be reported in (d).

was taken because the moving breather moves very slowly, as Fig. 10 indicates, if obtained by perturbing a discrete breather using the pinned mode.

References

[1] Y.I. Frenkel, T. Kontorova, Zh. Eksp. Teor. Fiz. 8 (1340) (1938).
[2] F.C. Frank, J.H. van der Merwe, Proc. R. Soc. Lond. Ser. A. Math. Phys. Sci. 198 (1053) (1949) 205–216.
[3] F.C. Frank, J. Van der Merwe, Proc. R. Soc. Lond. Ser. A. Math. Phys. Sci. 198 (1053) (1949) 216–225.
[4] F.C. Frank, J. Van der Merwe, Proc. R. Soc. Lond. Ser. A. Math. Phys. Sci. 200 (1060) (1949) 125–134.
[5] H. Mikeska, J. Phys. C: Solid State Phys. 13 (15) (1980) 2913.
[6] H.-J. Mikeska, M. Steiner, Adv. Phys. 40 (3) (1991) 191–356.
[7] G. Wysin, A. Bishop, P. Kumar, J. Phys. C: Solid State Phys. 18 (20) (1985) 4077.
[8] G. Wysin, A. Bishop, J. Oitmaa, J. Phys. C: Solid State Phys. 19 (2) (1986) 221.
[9] J. Krumhansl, J. Schrieffer, Phys. Rev. B 11 (9) (1975) 3535.
[10] T. Schneider, E. Stoll, Phys. Rev. B 13 (3) (1976) 1216.
[11] R. Cowley, G. Coombs, J. Phys. C: Solid State Phys. 6 (1) (1973) 143.
[12] W. Su, J. Schrieffer, A.J. Heeger, Phys. Rev. Lett. 42 (25) (1979) 1698.
[13] S. Yomosa, Phys. Rev. A 30 (1) (1984) 474.
[14] D. Chevizovich, D. Michieletto, A. Mvogo, F. Zakiryanov, S. Zdravković, R. Soc. Open Sci. 7 (11) (2020) 200774.
[15] M.T.A. Saif, J. Microelectromech. Syst. 9 (2) (2000) 157–170.
[16] M. Sulfridge, T. Saif, N. Miller, M. Meinhart, J. Microelectromech. Syst. 13 (5) (2004) 725–731.
[17] M. Vangbo, Sensors Actuators A 69 (3) (1998) 212–216.
[18] P. Cazottes, A. Fernandes, J. Pouget, M. Hafez, J. Mech. Des. 131 (10) (2009).
[19] N. Nadkarni, C. Daraio, D.M. Kochmann, Phys. Rev. E 90 (2) (2014) 023204.
[20] K. Bertoldi, V. Vitelli, J. Christensen, M. Van Hecke, Nat. Rev. Mater. 2 (11) (2017) 1–11.
[21] J.R. Raney, J.A. Lewis, Mrs Bull. 40 (11) (2015) 943–950.
[22] K. Bertoldi, P.M. Reis, S. Willshaw, T. Mullin, Adv. Mater. 22 (3) (2010) 361–366.
[23] H. Yasuda, J. Yang, Phys. Rev. Lett. 114 (18) (2015) 185502.
[24] Q. Wang, J.A. Jackson, Q. Ge, J.B. Hopkins, C.M. Spadaccini, N.X. Fang, Phys. Rev. Lett. 117 (17) (2016) 175901.
[25] R.H. Baughman, S. Stafstrom, C. Cui, S.O. Dantas, Science 279 (5356) (1998) 1522–1524.
[26] Y. Ding, Z. Liu, C. Qiu, J. Shi, Phys. Rev. Lett. 99 (9) (2007) 093904.
[27] R. Süsstrunk, S.D. Huber, Science 349 (6243) (2015) 47–50.
[28] B.G.-g. Chen, B. Liu, A.A. Evans, J. Paulose, I. Cohen, V. Vitelli, C. Santangelo, Phys. Rev. Lett. 116 (13) (2016) 135501.
[29] D. Rocklin, S. Zhou, K. Sun, X. Mao, Nature Commun. 8 (1) (2017) 1–9.
[30] Y. Cao, M. Derakhshani, Y. Fang, G. Huang, C. Cao, Adv. Funct. Mater. 31 (45) (2021) 2106231.
[31] D.M. Kochmann, K. Bertoldi, Appl. Mech. Rev. 69 (5) (2017).
[32] B. Haghpanah, L. Salari-Sharif, P. Pourrajab, J. Hopkins, L. Valdevit, Adv. Mater. 28 (36) (2016) 7915–7920.
[33] A. Rafsanjani, K. Bertoldi, A.R. Studart, Science Robotics 4 (29) (2019) eaav7874.
[34] S. Nishikawa, Y. Arai, R. Niiyama, Y. Kuniyoshi, IEEE Robot. Autom. Lett. 3 (2) (2018) 1018–1024.
[35] S.-P. Jung, G.-P. Jung, J.-S. Koh, D.-Y. Lee, K.-J. Cho, J. Mech. Robot. 7 (2) (2015) 021010.
[36] R.L. Harne, K. Wang, Smart Mater. Struct. 22 (2) (2013) 023001.
[37] M. Hwang, A.F. Arrieta, Smart Mater. Struct. 31 (1) (2021) 015021.
[38] M.I. Friswell, S.F. Ali, O. Bilgen, S. Adhikari, A.W. Lees, G. Litak, J. Intell. Mater. Syst. Struct. 23 (13) (2012) 1505–1521.
[39] S. Shan, S.H. Kang, J.R. Raney, P. Wang, L. Fang, F. Candido, J.A. Lewis, K. Bertoldi, Adv. Mater. 27 (29) (2015) 4296–4301.
[40] O.R. Bilal, A. Foehr, C. Daraio, Proc. Natl. Acad. Sci. 114 (18) (2017) 4603–4606.
[41] B. Deng, J. Raney, K. Bertoldi, V. Tournat, J. Appl. Phys. 130 (4) (2021) 040901.
[42] B. Deng, J. Raney, V. Tournat, K. Bertoldi, Phys. Rev. Lett. 118 (20) (2017) 204102.
[43] B. Deng, V. Tournat, P. Wang, K. Bertoldi, Phys. Rev. Lett. 122 (4) (2019) 044101.
[44] E.B. Herbold, V.F. Nesterenko, Phys. Rev. Lett. 110 (14) (2013) 144101.
[45] H. Yasuda, Y. Miyazawa, E.G. Charalampidis, C. Chong, P.G. Kevrekidis, J. Yang, Sci. Adv. 5 (5) (2019) eaau2835.
[46] S. Katz, S. Givli, Extreme Mech. Lett. 22 (2018) 106–111.
[47] M. Hwang, A.F. Arrieta, Phys. Rev. E 98 (4) (2018) 042205.
[48] H. Yasuda, L. Korpas, J. Raney, Phys. Rev. Appl. 13 (5) (2020) 054067.
[49] M. Hwang, A.F. Arrieta, Sci. Rep. 8 (1) (2018) 1–9.
[50] J.R. Raney, N. Nadkarni, C. Daraio, D.M. Kochmann, J.A. Lewis, K. Bertoldi, Proc. Natl. Acad. Sci. 113 (35) (2016) 9722–9727.
[51] N. Nadkarni, A.F. Arrieta, C. Chong, D.M. Kochmann, C. Daraio, Phys. Rev. Lett. 116 (24) (2016) 244501.
[52] L. Jin, R. Khajehtourian, J. Mueller, A. Rafsanjani, V. Tournat, K. Bertoldi, D.M. Kochmann, Proc. Natl. Acad. Sci. 117 (5) (2020) 2319–2325.
[53] H. Yasuda, H. Shu, W. Jiao, V. Tournat, J.R. Raney, Appl. Phys. Lett. 123 (5) (2023) 051701.
[54] M. Remoissenet, Phys. Rev. B 33 (4) (1986) 2386.
[55] S. Flach, A.V. Gorbach, Phys. Rep. 467 (1–3) (2008) 1–116.
[56] R. MacKay, S. Aubry, Nonlinearity 7 (6) (1994) 1623.
[57] S. Aubry, T. Cretegny, Physica D 119 (1–2) (1998) 34–46.
[58] D. Chen, S. Aubry, G.P. Tsironis, Phys. Rev. Lett. 77 (1996) 4776–4779.
[59] S. Flach, C.R. Willis, Phys. Rep. 295 (5) (1998) 181–264.
[60] H. Duran, J. Cuevas-Maraver, P.G. Kevrekidis, A. Vainchtein, Commun. Nonlinear Sci. Numer. Simul. 111 (2022) 106435.
[61] J. Cuevas, F. Palmero, J. Archilla, F. Romero, Phys. Lett. A 299 (2–3) (2002) 221–225.
[62] A.V. Gorbach, M. Johansson, Phys. Rev. E 67 (6) (2003) 066608.
[63] A. Alvarez, F. Romero, J. Cuevas, J. Archilla, Phys. Lett. A 372 (8) (2008) 1256–1264.
[64] A. Alvarez, F. Romero, J. Cuevas, J.F. Archilla, Eur. Phys. J. B 70 (4) (2009) 543–555.
[65] S. Dmitriev, P. Kevrekidis, B. Malomed, D. Frantzeskakis, Phys. Rev. E 68 (5) (2003) 056603.
[66] S.V. Dmitriev, D.A. Semagin, A.A. Sukhorukov, T. Shigenari, Phys. Rev. E 66 (4) (2002) 046609.
[67] A. Maluckov, L. Hadžievski, M. Stepić, Eur. Phys. J. B 53 (3) (2006) 333–341.
[68] I.E. Papacharalampous, P.G. Kevrekidis, B.A. Malomed, D.J. Frantzeskakis, Phys. Rev. E 68 (2003) 046604.
[69] S.V. Dmitriev, D.J. Frantzeskakis, Solitary wave collisions, in: The Discrete Nonlinear SchrÖDinger Equation: Mathematical Analysis, Numerical Computations and Physical Perspectives, Springer Berlin Heidelberg, Berlin, Heidelberg, 2009, pp. 311–327.
[70] Z. Wu, Y. Zheng, K. Wang, Phys. Rev. E 97 (2) (2018) 022209.
[71] Z. Wu, K.-W. Wang, J. Sound Vib. 458 (2019) 389–406.
[72] A. Porubov, Int. J. Non-Linear Mech. 137 (2021) 103788.

[73] K.J. Moore, J. Bunyan, S. Tawfick, O.V. Gendelman, S. Li, M. Leamy, A.F. Vakakis, Phys. Rev. E 97 (1) (2018) 012219.
[74] M.M. Lee, E.G. Charalampidis, S. Xing, C. Chong, P.G. Kevrekidis, Phys. Rev. E 107 (2023) 054208.
[75] H. Duran, J. Cuevas-Maraver, P.G. Kevrekidis, A. Vainchtein, Phys. Rev. E 107 (2023) 014220.
[76] S. Katz, S. Givli, Phys. Rev. E 100 (3) (2019) 032209.
[77] B. Deng, P. Wang, V. Tournat, K. Bertoldi, J. Mech. Phys. Solids 136 (2020) 103661.
[78] H. Yasuda, E.G. Charalampidis, P.K. Purohit, P.G. Kevrekidis, J.R. Raney, Phys. Rev. E 104 (5) (2021) 054209.
[79] J. Meaud, K. Che, Int. J. Solids Struct. 122 (2017) 69–80.
[80] J. Marín, S. Aubry, Physica D 119 (1–2) (1998) 163–174.